Surface Microscopic Structure and Electrochemical Rectification of a Branched Alkanethiol Self-Assembled Monolayer

ARTICLE *in* THE JOURNAL OF PHYSICAL CHEMISTRY B · FEBRUARY 2006

Impact Factor: 3.3 · DOI: 10.1021/jp056356k · Source: PubMed

3 AUTHORS, INCLUDING:

Qijin Chi
Technical University of Denmark
100 PUBLICATIONS **2,308** CITATIONS
SEE PROFILE

Jingdong Zhang
Technical University of Denmark
100 PUBLICATIONS **2,309** CITATIONS
SEE PROFILE

THE JOURNAL OF PHYSICAL CHEMISTRY B LETTERS

2006, *110,* 1102−1106
Published on Web 12/24/2005

Surface Microscopic Structure and Electrochemical Rectification of a Branched Alkanethiol Self-Assembled Monolayer

Qijin Chi,* Jingdong Zhang, and Jens Ulstrup*

Department of Chemistry and NanoDTU, Technical University of Denmark, DK-2800 Kgs, Lyngby, Denmark

Received: November 3, 2005; In Final Form: December 13, 2005

The *tert*-butanethiol self-assembled monolayers (SAMs) on Au(111) surfaces were prepared from various solvents and investigated by a combination of scanning tunneling microscopy (STM) and electrochemistry in aqueous environments. High-resolution STM images reveal a $(\sqrt{7} \times \sqrt{7})$R19° surface lattice structure, in contrast with the conventional lattice $(\sqrt{3} \times \sqrt{3})$R30° structure for straight-chain alkanethiol SAMs. Interestingly, such a branched monolayer shows electrochemical rectification toward redox probes. We suggest that electrochemical rectification could be a general characteristic of short-chain branched alkanthiol SAMs, and originate in localized electronic effects.

1. Introduction

Self-assembled monolayers (SAMs) on various substrates, particularly thiol-gold based SAMs, have offered versatile pathways towards functionalization of surfaces and/or interfaces for molecular electronics applications.[1,2] Future advance of this field is anticipated to rest on rational design and control of SAMs with "smart" functions. Besides synthesis of new materials, this goal has increasingly demanded fundamental insight into electronic structures and interfacial properties of the SAMs at the nanoscale and single-molecule levels, where a number of both experimental and theoretical efforts have already been made.[2] Scanning tunneling microscopy (STM) has shown notable advantages to resolve assembly dynamics, phase transitions, and electronic structures of many SAMs in both ultrahigh vacuum (UHV)[3−5] and aqueous[6−8] environments. One recent development is to combine electrochemistry and in situ STM in detailed characterization of SAMs at liquid/solid interfaces crucial for bioelectronic applications (e.g., immobilization of redox proteins and their electronic coupling with the specific SAM).[9−14] We here present interesting observations of surface lattice structure and charge-transfer behavior toward redox probes for a short-chain branched alkanethiol, i.e., *tert*-butanethiol (with three terminal methyl groups) monolayer. The surface electronic structure and other interfacial properties of this SAM are compared with those of two reference systems, i.e., 1-propanethiol and 1-decanethiol monolayers.

Compared to long-chain (the number of methylene groups $n \geq 10$) alkanethiol SAMs, surface structural features of very short-chain ($n \leq 4$) thiol SAMs are less explored and with notable uncertainty. This arises from structural diversity and flexibility in the spontaneous formation of short-chain SAMs. In the present case, the solvent effect on the monolayer structures is significant. A comparison of the quality of *tert*-butanethiol monolayers prepared from water, ethanol, water−ethanol mixture (1:1, v/v), and tetrahydrofuran shows that the most compact and ordered monolayers are those prepared from water, although the saturated surface coverage of *tert*-butanethiol assembled from the four solvents is virtually the same. Solvent effects could thus play a crucial role in determining surface packing of *tert*-butanethiol molecules. All results and discussions below are therefore based on monolayers prepared from water.

2. Experimental Section

The Au(111) substrates used in both electrochemical and STM experiments were homemade as previously.[15,16] *tert*-Butanethiol (also named *tert*-butylmercaptan, $(CH_3)_3CSH$, 98.5%), 1-propanethiol ($CH_3CH_2CH_2SH$, 99%), 1-decanethiol ($CH_3(CH_2)_9SH$, 96%), and tetrahydrofuran (THF, 99.9%) from Sigma-Aldrich were used as received. $K_4Fe(CN)_6 \cdot 3H_2O$ (>99%) and $K_3Fe(CN)_6$ (>99%) from Merck were used without further purification. Tris(1,10-phenanthroline) cobalt(III) perchlorate ($Co(phen)_3(ClO_4)_3 \cdot 2H_2O$) was synthesized from $CoCl_2$, 1,10-phenanthroline, perchloric acid, and bromine according to reported procedures.[17] Absolute ethanol (ultrapure) was from Merck. The NH_4Ac buffer (5 mM, pH 4.6) was prepared from 5 M stock solution (Fluka, ultrapure) and solution pH adjusted with acetic acid (Aldrich, 99.7%). This buffer was chosen for the present study because of its advantages for exploring long-range interfacial ET of blue copper protein azurin immobilized on the alkanethiol-modified Au(111) electrodes. NaOH (0.5 M) solutions prepared from 30% stock solutions (ultrapure, Merck) were used in voltammetric measurements of reductive desorption. Milli-Q water (18.2 MΩ) was used throughout.

The SAMs of alkanethiols were prepared by immersing freshly quenched Au(111) electrodes in an appropriate solvent containing the alkanethiol (1−5 mM) overnight, followed by thorough rinsing with ethanol and Milli-Q water before measurements. Electrochemical experiments were carried out using an Autolab system (Eco Chemie, Netherlands), with a three-electrode system consisting of a Pt counter electrode, a reversible hydrogen electrode (RHE) as the reference electrode, and an

* Corresponding authors. E-mail: cq@kemi.dtu.dk (Q.C.) and ju@kemi.dtu.dk (J.U.).

10.1021/jp056356k CCC: $33.50

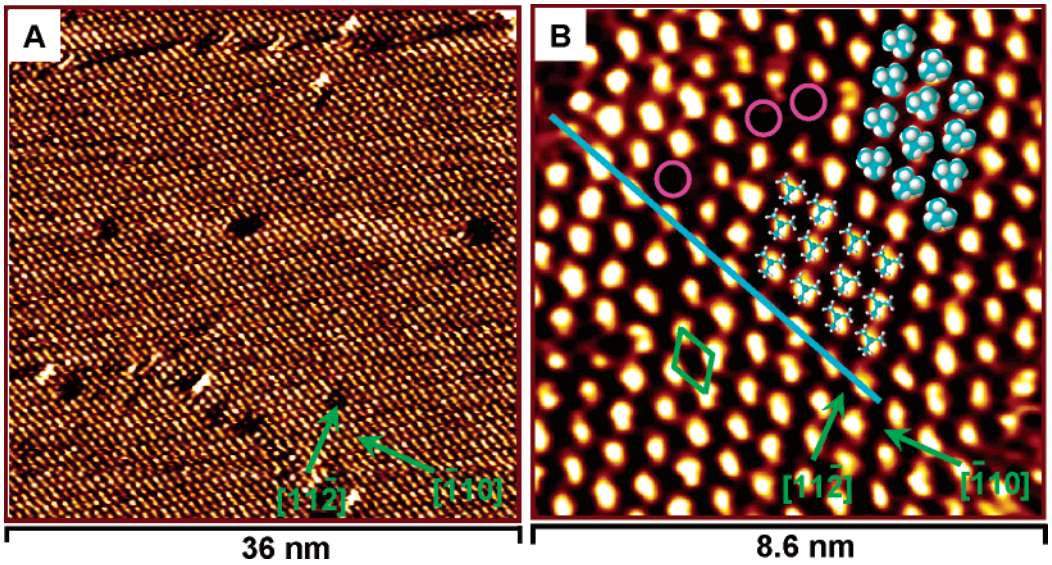

Figure 1. Electrochemical STM images of *tert*-butanethiol monolayer/Au(111) acquired in an NH_4Ac buffer (pH 4.6) in the constant current mode. Scan area (A) 36 × 36 and (B) 8.6 × 8.6 nm^2, $I_t = 0.12$ nA, $V_{bias} = -0.2$ V, $E_w = -0.12$ V (vs SCE). The lattice directions, a unit cell, and *tert*-butanethiol molecules represented by space-filling and ball-and-stick models are added in the STM images.

Au(111)-based working electrode. All potentials are reported versus SCE. STM imaging was performed using a PicoSPM system (Molecular Imaging Co.) equipped with a bipotentiostat for potential control of both the substrate and tip. Electrochemical control in STM was conducted in a home-designed cell with a three-electrode system similar to electrochemical measurements. The tips were prepared from either tungsten or Pt/Ir (80:20) wire by electrochemical etching and insulated with Apiezon wax to suppress Faradaic currents to a 10 pA level or less. All images were acquired in the constant current mode under potential control where the potential range of the sample substrate was set in a suitable region (e.g., −0.2 to +0.4 V vs SCE) in which neither reductive nor oxidative desorption of the SAMs would occur during the STM imaging.

3. Results and Discussion

STM images demonstrate that the *tert*-butanethiol monolayer is composed of large ordered domains (≥100 nm) with few boundaries over the whole surface. Both size and density of pinholes or defects, a common surface structural feature of alkanethiol SAMs on Au(111), are much smaller and lower than SAMs consisting of either 1-propanethiol or 1-decanethiol observed under the same or similar experimental conditions. STM measurements focused on ordered domains disclose detailed structural information. Figure 1 shows two representative STM images from such observations. The molecules are organized along certain directions to form a periodic lattice structure, but the arrangement follows neither the atomic row [$\bar{1}$10] of the Au(111) surface nor the[11$\bar{2}$] direction perpendicular to the atomic row. Instead, there is a 19° (±2°) angle between the molecular rows and the Au(111) atomic rows (Figure 1B), and the distance between the nearest neighbor molecules is 7.5 (±0.3) Å. The unit cell can best be assigned as $(\sqrt{7} \times \sqrt{7})$R19° with an inside angle of 60° or 120° (Figure 1B), and this lattice structure corresponds to a surface coverage of 3.3×10^{-10} mol·cm^{-2} (equivalent to $\theta = 0.14$).

Reductive desorption is one of the most striking features of the gold−sulfur based SAMs and has been used to characterize the monolayer properties and to estimate the sulfur coverage. Electrochemical voltammetry has offered a straightforward way to disclose this feature.[6,18−21] Furthermore, a combination of

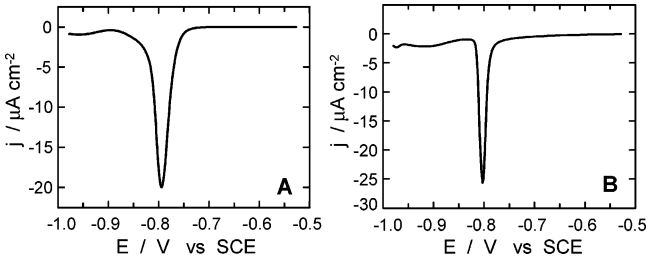

Figure 2. Linear scan voltammograms of reductive desorption for (A) 1-propanethiol-monolayer/Au(111), and (B) *tert*-butanethiol-monolayer/Au(111) electrodes in 0.5 M NaOH solution. Scan rate, 10 mV s^{-1}.

electrochemical measurements and STM analysis allows one to reveal detailed surface structures of the SAMs at liquid/solid interfaces.[6] As an example of the present case, linear scan voltammograms of 1-propanethiol- and *tert*-butanethiol monolayers are compared in Figure 2. Well-defined cathodic peaks are observed for both monolayers. The peak potential and the Faradaic charge of the reductive desorption for the 1-propanethiol SAM are fully as expected, and the system can therefore serve as an effective reference. The cathodic peak of the *tert*-butanethiol monolayers is always negatively shifted by ca. 20 mV compared to that for 1-propanethiol, although the *tert*-butanethiol SAM is shorter by a methylene unit. It is well-known for straight-chain alkanethiols that the reductive potential is shifted negatively on elongating the alkyl chain (≈15 mV negative shift per methylene unit).[9,18,21] Thus, the present observation could imply that the sulfur−gold bond is stronger than for the conventional case, likely resulting from the contribution of three terminal methyl groups. In addition, the reductive desorption peak of *tert*-butanethiol is notably sharper than that of 1-propanethiol. This is consistent with only one dominant conformation existing in the *tert*-butanethiol monolayer, as revealed in the STM image (Figure 1B).

The surface coverage of *tert*-butanethiol estimated from electrochemical reductive desorption (e.g., Figure 2B) is 3.6 (±0.5) × 10^{-10} mol·cm^{-2}, largely consistent with the STM analysis. We thus conclude that each unit contains one molecule, and each bright spot in the STM images (e.g., Figure 1B) represents one molecule. This is further supported by analyses of defect sites within the ordered domains, regarded as "missing"

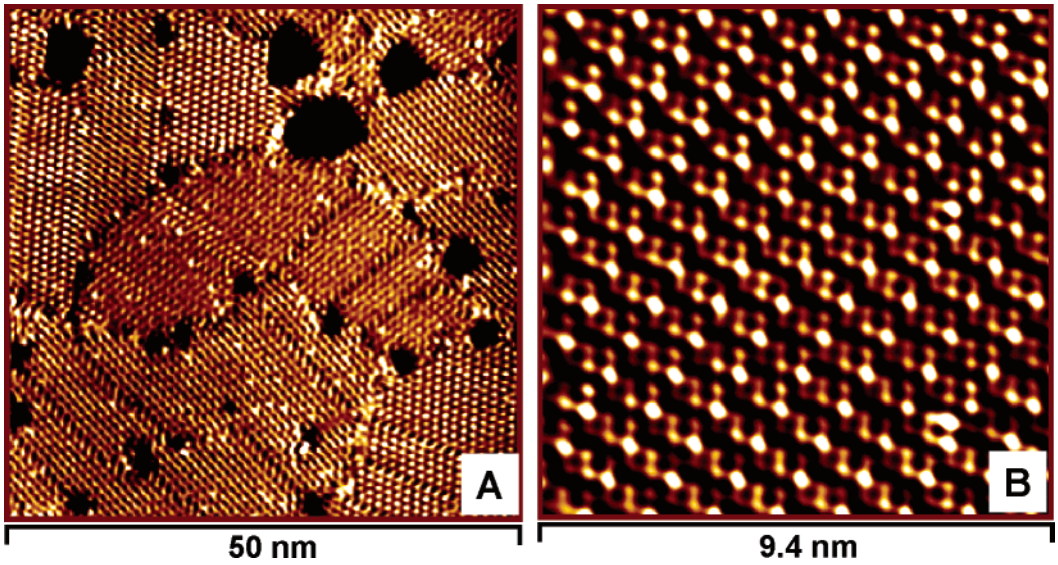

Figure 3. Electrochemical STM images of 1-propanethiol monolayer/Au(111) acquired in an NH_4Ac buffer (pH 4.6) in the constant current mode. Scan area (A) 50 × 50 and (B) 9.4 × 9.4 nm^2, $I_t = 0.21$ nA, $V_{bias} = -0.10$ V, $E_w = -0.15$ V (vs SCE).

molecules (three missing molecules in Figure 1B are marked by pink circles).[6] Such a surface lattice structure is in remarkable contrast with the "classic" lattice ($\sqrt{3} \times \sqrt{3}$)R30° or ($2\sqrt{3} \times 3$)R30°-4 structures of alkanethiol SAMs with one terminal methyl group. We also notice that all bright spots (most likely reflecting the sulfur heads of *tert*-butanethiol molecules) are not strictly aligned on one line, but with a zigzag caused by a certain deviation in every other row. Such an arrangement is most likely driven by hydrophobic interactions among terminal methyl groups of neighboring molecules, enabling to optimize molecular organization with the most compact character. Rational simulations of STM images using density functional theory (DFT) and/or molecular dynamics (MD) are in attempt, and could help to better understand the physical/chemical nature of the monolayer organization.

As a comparison, high-resolution STM images for 1-propanethiol monolayers (Figure 3) were acquired and analyzed similarly. The monolayer has an expected ($2\sqrt{3} \times 3$)R30°-4 lattice structure. Interestingly, a unit cell is composed of one molecule with stronger contrast and three molecules with weaker contrast. These observations suggest that there are two dominant conformations coexisting in the 1-propanethiol monolayer, correspondingly illustrated by two kinds of significantly different contrast (Figure 3B). We have previously proposed a possible mechanism to account for different contrasts.[6,13]

Interfacial properties of various SAMs can be elucidated using small redox couples as probes.[16,22−29] In particular, Takehara et al. have performed systematic studies on interactions between the SAMs with hydrophilic headgroups and redox species, and they found that electrostatic effects determined crucially the interfacial electron transfer (ET) rate of redox probes.[26] The most common redox probes for aqueous environment are $[Fe(CN)_6]^{3-/4-}$ and $[Ru(NH_3)_6]^{3+/2+}$ couples, due to their water solubility and excellent redox behavior. The choice of appropriate redox probes, however, also depends on the available potential window of the specific SAM, in which neither reductive nor oxidative desorption should be involved. In the present case, the SAMs have a short chain and thus only a relatively narrow potential range can be applied. $[Fe(CN)_6]^{3-/4-}$ and $[Co(phen)_3]^{3+/2+}$ couples are proven as the most suitable redox probes in this study.

Figure 4 shows a comparison of cyclic voltammograms (CVs) at different electrodes in the presence of 5 mM $K_4Fe(CN)_6$ in

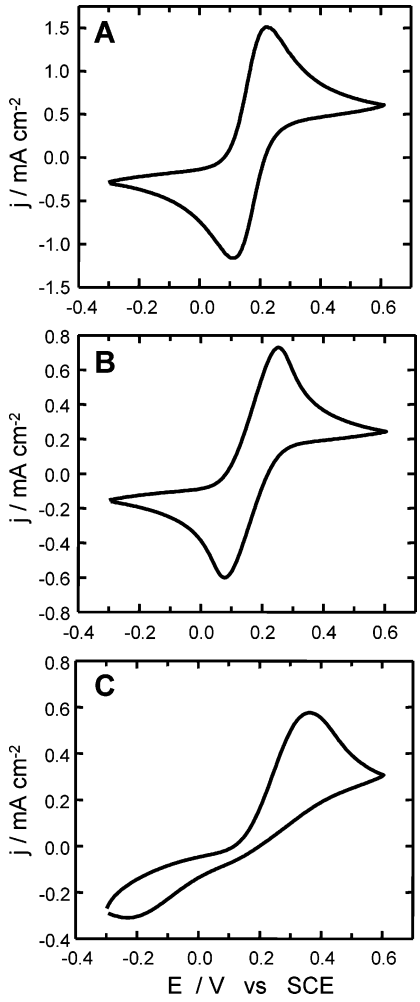

Figure 4. Cyclic voltammograms of (A) bare Au(111), (B) 1-propanethiol-monolayer/Au(111), and (C) *tert*-butanethiol-monolayer/Au(111) electrodes in an NH_4Ac buffer (pH 4.6) containing 5 mM $K_4Fe(CN)_6$. Scan rate 50 mV s^{-1}.

electrolyte solutions. As expected, the redox reaction is quasi-reversible at a bare Au(111) electrode, with symmetric cathodic and anodic currents (Figure 4A). The presence of 1-propanethiol monolayer film reduces the Faradaic currents and slows down

the kinetics as indicated by increasing peak separation, but the voltammogram largely remains symmetric (Figure 4B). In both cases the electrochemical process is diffusion-controlled, as confirmed by a linear relation between the peak current and the square root of the scan rate (Supporting Information, Figure S1). Voltammetric measurements were also performed at 1-decanethiol modified Au(111) electrodes (data not shown), in which no Faradaic current is detectable. As previously observed,[22] interfacial electron transfer (ET) is completely blocked or this long-chain monolayer serves well as an insulating film under the present conditions. In striking contrast, the presence of a *tert*-butanethiol monolayer results in a strongly asymmetric flow of the Faradaic currents, with the cathodic current largely suppressed (Figure 4C). This phenomenon can be termed "electrochemical rectification". It is noted that none of the CVs in Figure 4 depend on the potential scan direction. The anodic peak current is proportional to the square root of the scan rate, but significant deviations from the linear relation were observed at modest to high scan rates (>120 mV s^{-1}) (Supporting Information, Figure S1). Furthermore, similar voltammetric behavior is observed under three conditions: (a) 5 mM $[Fe(CN)_6]^{4-}$, (b) 2.5 mM $[Fe(CN)_6]^{4-}$ + 2.5 mM $[Fe(CN)_6]^{3-}$, and (c) 5 mM $[Fe(CN)_6]^{3-}$. This clearly indicates that voltammetric behavior is independent of the initial redox state of the redox probe. To test possible effects of electrolyte type and solution pH, similar measurements were performed in 0.1 M $HClO_4$ (pH 1.1) containing $[Fe(CN)_6]^{3-/4-}$. The results are qualitatively similar, with electrochemical rectification observed only at *tert*-butanethiol monolayer modified electrodes (Supporting Information, Figure S2). We carried out further investigations with a positively charged redox probe, tris(1,10-phenanthroline) cobalt(III) ($[Co(phen)_3]^{3+}$). This redox probe exhibits well-defined voltammetric behavior at both bare and 1-propanethiol-modified Au(111) electrodes (Supporting Information, Figure S3A and B). The asymmetric redox feature is observed at *tert*-butanethiol monolayer modified electrodes (Supporting Information, Figure S3C) but is much less profound than for $[Fe(CN)_6]^{3-/4-}$.

We can thus summarize experimental observations at *tert*-butanethiol monolayer modified Au(111) electrodes briefly: (1) electrochemical rectification can be observed for both negatively and positively charged redox probes; (2) the extent of electrochemical rectification is related to physical/chemical properties of the redox probes (e.g., charge state and hydrophobicity), but it appears to be independent of the initial redox state; (3) the degree of electrochemical rectification could also be affected by the electrolyte type and solution pH, which arguably interfere with microscopic structures of the SAMs.

Asymmetric voltammetry (or electrochemical rectification) toward a redox probe was previously observed and represented by two cases.[16,28] However, the SAM in those two cases contained a redox moiety, i.e., ferrocene covalently attached to the alkanethiol[28] or the copper center in an azurin molecule,[16] making the monolayer itself electrochemically active. With redox mediation, electrochemical rectification in these two cases follows a mechanism similar to electrocatalysis observed at many redox-polymer-modified electrodes.[30,31]

The present system is significantly different, because there is no redox species in the *tert*-butanethiol monolayer. The robust, although different-extent redox rectification for both $[Fe(CN)_6]^{3-/4-}$ and $[Co(phen)_3]^{3+/2+}$ couples is thus in contrast to both the straight alkanethiols, i.e., the short alkanethiol (1-propanethiol) with symmetric voltammograms and the long alkanethiol (1-decanethiol) which blocks voltammetric response completely. There is no straightforward interpretation of such effects, but voltammetric asymmetry, or "rectification" resembling the observations above has in fact been observed in other cases.[26] The following different molecular mechanisms can be envisaged: (a) The electroactive species could diffuse, or percolate, through defects or pinholes in the monolayer film. This effect could be more pronounced for the voluminous branched alkanethiol than for the short straight-chain alkanethiol. Percolation could also be expected to be more facile for the hydrophobic $[Co(phen)_3]^{3+/2+}$ couple with the smaller voltammetric asymmetry than for the hydrophilic $[Fe(CN)_6]^{3-/4-}$ couple with stronger asymmetry. There are, however, two reservations to this suggestion. One is that the *tert*-butanethiol SAM is in fact more densely packed. Pinholes would therefore have to be of "dynamic", transient character. The other reservation is that diffusion/percolation of the more highly charged, reduced $[Fe(CN)_6]^{4-}$ form would appear more facile than the oxidized $[Fe(CN)_6]^{3-}$ form. There is some evidence for more extensive and selective ion pairing of $[Fe(CN)_6]^{4-}$ compared with $[Fe(CN)_6]^{3-}$.[32] Preferential percolation of less charged $M_x[Fe(CN)_6]^{(4-x)-}$ ($x > 1$, M = alkali metal ion) would thus have to be invoked as an additional feature of the observed electrochemical rectification. (b) Localized electronic surface states associated with the Au−S binding unit have been suggested as a rationale for observed electronic Raman scattering at roughened Au and Ag surfaces covered by long-chain alkanethiols.[33] A certain length (>8 methylene units) for alkanethiols is required, but this could be matched by shorter branched (vs straight) alkanethiols. Au−S based electronic surface states dominate the Au−S headgroup surface region but would not have to act as real redox centers in order to induce interfacial ET rectification. As long as the surface state is energetically well below the solvent environmental "band" states, rectification can instead be assigned to the electronic tunneling factor in a superexchange mode through the localized surface state. In this context, the "rectification ratio" can be significant and amount to a factor from 2 for the $[Co(phen)_3]^{3+/2+}$ couple and a factor of about 5 for the $[Fe(CN)_6]^{3-/4-}$ couple. This suggests that the effect is not rooted in activation energy difference, which could give rise to rectification ratios of orders of magnitude.

The superexchange electronic factor for tunneling between the molecule ("mol") and the electrode ("el") through a single intermediate electronic state ("s") is[34]

$$V_{\mathrm{mol,el}} = \frac{V_{\mathrm{mol,s}} V_{\mathrm{s,el}}}{\Delta E(\eta)} \tag{1}$$

where the V values are the electronic couplings between the states indicated by the subscripts and the energy gap ($\Delta E(\eta)$) between the surface state and the donor ($[Fe(CN)_6]^{4-}$, $[Co(phen)_3]^{2+}$), or acceptor ($[Fe(CN)_6]^{3-}$, $[Co(phen)_3]^{3+}$) molecular state for the anodic and cathodic process, respectively. The asymmetry of the cathodic (c) and anodic (a) current ($j_{c,a}$) is then represented by the explicit dependence of the energy gap ($\Delta E(\eta)$) on the overpotential (η) and follows[35]

$$j_{\mathrm{c,a}} \propto \left|\frac{V_{\mathrm{mol,s}} V_{\mathrm{s,el}}}{\Delta E(\eta)}\right|^2 \tag{2}$$

The electrochemical potential of the surface state is most likely to follow largely the Au(111)-electrode potential. It can then be shown that the energy gap increases with increasing cathodic overpotential, but decreases with increasing anodic overpotential. This gives rise to electronic asymmetry in the direction observed,

i.e., a larger current in the anodic direction than in the cathodic direction. The absolute value of the current ratio depends on the energy gap of the surface state above the Fermi energy of the Au(111)-electrode. For this rationale to hold, furthermore, the energy of the surface state would have to be lower for *tert*-butanethiol than for 1-propanethiol. Such information could become available by computational approaches such as reported recently.[13]

In summary, *tert*-butanethiol is a very short branched alkanethiol with three terminal methyl groups. Strong hydrophobic interactions among the terminal groups appear to play a dominant role in the molecular packing, which induces assembly into a densely packed monolayer on Au(111) with few defects. This differs dramatically from the short-chain straight alkanethiol reference system (e.g., 1-propanethiol). Most interestingly, such a branched monolayer film can invoke electrochemical rectification toward redox probes. We suggest that electrochemical rectification originates in an asymmetric electronic effect, although the details of the exact mechanism remain open. These findings could offer information of interest in rational design of SAMs for molecular electronics. The system could also serve as a suitable example for theoretical modeling of the surface structures and interfacial properties of Au−S bonded SAMs.

Acknowledgment. This work was supported by the Danish Technical Science Research Council, presently renamed as the Danish Research Council for Technology and Production.

Supporting Information Available: Additional electrochemical results under various experimental conditions: Figure S1 showing relationship between anodic peak currents and scan rates obtained at bare, 1-propanethiol-modified, and *tert*-butanethiol-modified Au(111) electrodes in a NH_4Ac buffer (pH 4.6) containing 5 mM $K_4Fe(CN)_6$; Figure S2 showing cyclic voltammograms of 5 mM $K_4Fe(CN)_6$ in 0.1 M $HClO_4$ for three kinds of electrodes; and Figure S3 showing cyclic voltammograms of 1.5 mM $[Co(phen)_3]^{3+}$ in a NH_4Ac buffer (pH 4.6) for three kinds of electrodes. This material is available free of charge via the Internet at http://pubs.acs.org.

References and Notes

(1) Fendler, J. H. *Chem. Mater.* **2001**, *13*, 3196−3210.
(2) Love, J. C.; Estroff, L. A.; Kriebel, J. K.; Nuzzo, R. G.; Whitesides, G. M. *Chem. Rev.* **2005**, *105*, 1103−1169.
(3) Poirier, G. E. *Chem. Rev.* **1997**, *97*, 1117−1127.
(4) Schreinber, F. *Prog. Surf. Sci.* **2000**, *65*, 151−256.
(5) Yang, G.; Liu, G.-Y. *J. Phys. Chem. B* **2003**, *107*, 8746−8759.
(6) Zhang, J.; Chi, Q.; Nielsen, J. U.; Friis, E. P.; Andersen, J. E. T.; Ulstrup, J. *Langmuir* **2000**, *16*, 7229−7237.
(7) Esplandiú, M. J.; Hagenström, H.; Kolb, D. M. *Langmuir* **2001**, *17*, 828−838.
(8) Ou Yang, L.-Y.; Yau, S.-L.; Itaya, K. *Langmuir* **2004**, *20*, 4596−4603.
(9) Chi, Q.; Zhang, J.; Andersen, J. E. T.; Ulstrup, J. *J. Phys. Chem. B* **2001**, *105*, 4669−4679.
(10) Zhang, J.; Chi, Q.; Hansen, A. G.; Wackerbarth, H.; Christensen, H. E. M.; Andersen, J. E. T.; Ulstrup, J. *J. Phys. Chem. B* **2002**, *106*, 1131−1152.
(11) Zhang, J.; Welinder, A. C.; Hansen, A. G.; Christensen, H. E. M.; Ulstrup, J. *J. Phys. Chem. B* **2003**, *107*, 12480−12484.
(12) Zhang, J.; Christensen, H. E. M.; Ooi, B. L.; Ulstrup, J. *Langmuir* **2004**, *20*, 10200−10207.
(13) Zhang, J.; Bilic, A.; Reimers, J. R.; Hush, N. S.; Ulstrup, J. *J. Phys. Chem. B* **2005**, *109*, 15355−15367.
(14) Chi, Q.; Farver, O.; Ulstrup, J. *Proc. Natl. Acad. Sci. U.S.A.* **2005**, *102*, 16203−16208.
(15) Chi, Q.; Zhang, J.; Friis, E. P.; Abdersen, J. E. T.; Ulstrup, J. *Electrochem. Commun.* **1999**, *1*, 91−96.
(16) Chi, Q.; Zhang, J.; Friis, E. P.; Chorkendorff, Ib; Canters, G. W.; Andersen, J. E. T.; Ulstrup, J. *J. Am. Chem. Soc.* **2000**, *122*, 4047−4055.
(17) Baker, B. P.; Basolo, F.; Neumann, H. M. *J. Phys. Chem.* **1959**, *63*, 371−378.
(18) Widrig, C. A.; Chung, C.; Porter, M. D. *J. Electroanal. Chem.* **1991**, *310*, 335−359.
(19) Zhong, C. J.; Porter, M. D. *J. Am. Chem. Soc.* **1994**, *116*, 11616−11617.
(20) Zhong, C. J.; Brush, R. C.; Anderegg, J.; Porter, M. D. *Langmuir* **1999**, *15*, 518−525.
(21) Imabayashi, S.-I.; Iida, M.; Hobara, D.; Feng, Z.-Q.; Niki, K.; Kakiuchi, T. *J. Electroanal. Chem.* **1997**, *428*, 33−38.
(22) Porter, M. D.; Bright, T. B.; Allara, D. L.; Chidsey, C. E. D. *J. Am. Chem. Soc.* **1987**, *109*, 3559−3568.
(23) Miller, C.; Cuendet, P.; Grätzel M. *J. Phys. Chem.* **1991**, *95*, 877−886.
(24) Miller, C.; Grätzel M. *J. Phys. Chem.* **1991**, *95*, 5225−5233.
(25) Becka, A. M.; Miller, C. J. *J. Phys. Chem.* **1992**, *96*, 2657−2668.
(26) Takehara, K.; Takemura, H.; Ide, Y. *Electrochim. Acta* **1994**, *39*, 817−822.
(27) Campbell, D. J.; Herr, B. R.; Hulteen, J. C.; Van Duyne, R. P.; Mirkin, C. A. *J. Am. Chem. Soc.* **1996**, *118*, 10211−10219.
(28) Alleman, K. S.; Weber, K.; Creager, S. E. *J. Phys. Chem.* **1996**, *100*, 17050−17058.
(29) Chi, Y.-S.; Hwang, S.; Lee, B. S.; Kwak, J.; Coi, I. S.; Lee, S.-G. *Langmuir* **2005**, *21*, 4268−4271.
(30) Andrieux, C. P.; Saveant, J. M. In *Molecular Design of Electrode Surfaces*; Murray, R. W., Ed.; Wiley: New York, 1992; Vol. 22, p 207.
(31) Majda, M. In *Molecular Design of Electrode Surfaces*; Murray, R. W., Ed.; Wiley: New York, 1992; Vol. 22, p 427.
(32) Scherer, G.; Willig, F. *J. Electroanal. Chem.* **1977**, *85*, 77−100.
(33) Gregory, B. W.; Clark, B. K.; Standard, J. M.; Avila, A. *J. Phys. Chem. B* **2001**, *105*, 4684−4689.
(34) Kuznetrov, A. M.; Ulstrup, J. *Electron Transfer in Chemistry and Biology: An Introduction to the Theory*; Wiley: Chichester, U.K., 1999.
(35) Marcus, R. A. *J. Chem. Soc., Faraday Trans.* **1996**, *92*, 3905−3908.